12-2016

Radar Detection of Tornadogenesis

Kristofer S. Tuftedal
Iowa State University, kristofer.tuftedal@stonybrook.edu

Radar Detection of Tornadogenesis

Kristofer S. Tuftedal

Department of Geological and Atmospheric Sciences, Iowa State University, Ames, Iowa

Dr. James V. Aanstoos

Department of Geological and Atmospheric Sciences, Iowa State University, Ames, Iowa

ABSTRACT

This research compared the basic and polarimetric radar products of non-tornadic and pre-tornadic supercells with the intent of finding a signature which appears to be indicative of tornadogenesis or a lack thereof. Reflectivity (Z_{HH}), spectrum width (σ_v), differential reflectivity (Z_{DR}), correlation coefficient (ρ_{hv}), and specific differential phase (K_{DP}) were all visually analyzed using GR2Analyst and compared to existing schematics in an attempt to find a signature. Once an apparent signature was found, pooled t-tests were performed on the data to see if the mean value of the pre-tornadic supercell, where the signature was found, had a statistically significant difference with the mean value of the non-tornadic supercell in the same area. Overall, it was found that the discovered signature was statistically significant on the 95% confidence level. However, due to the small number of cases tested, a relationship between the signature and tornadogenesis cannot be proven, but can be suggested.

---

1. Introduction and Background

Finding ways to more accurately forecast tornadogenesis has been a long-standing issue for National Weather Service (NWS) meteorologists. Issuing tornado warnings for supercells that do not produce tornadoes leads to the public believing that most tornado warnings are only false alarms, resulting in a sort of "crying wolf" effect. These false alarms not only harm the public's perception of the NWS, but could also potentially lead to serious injury to or even death of an individual that ignores a tornado warning due to their mistrust from previous warnings that did not produce a tornado.

Certain radar signatures have been found to be suggestive or indicative of tornadic activity, such as the tornado vortex signatures (TVS) and the tornado debris signatures (TDS) (Stelten and Wolf 2014). These signatures are either limited to moments prior to tornadogenesis like a TVS, or while a tornado is ongoing like a TDS. While these signatures are highly useful in their own respects, such as determining whether a supercell has enough vertical vorticity to produce a tornado or showing that a tornado

is ongoing and is lofting debris without having to rely on trained spotters, the public, or law enforcement to confirm this, these signatures do little to aid a meteorologist in determining whether a supercell will become tornadic in advance of tornadogenesis.

Dual-polarization (Polarimetric) radar is a relatively new tool in the world of Doppler radar. Even though the first research polarimetric radar was installed in 1983 and the first collection of polarimetric variables became available in 1992; the upgrade of the Weather Surveillance Radar-1988 Doppler (WSR-88D) radars ran by NWS was not completed until 2013. Hence, we are only beginning to understand the operational potential that polarimetric products have to offer.

Some early research into detecting tornadoes with polarimetric products was done in Ryzhkov et al. (2005). That study looked at different radar products, both polarimetric and not. The study looked at reflectivity factor (Z_{HH}), radial velocity, differential reflectivity (Z_{DR}), specific differential phase (K_{DP}), and correlation coefficient (ρ_{hv}) in order to determine the usefulness of these products in tornado detection. That research, while showing that polarimetric data was definitely capable of detecting ongoing tornadoes and would help forecasters with issuing tornado warnings, also found polarimetric signatures aloft and near the supercells in the study. These signatures were deemed as out of the ordinary and that they could be related with the tornadogenesis processes. The signatures referred as out of the ordinary in that study were not explicitly mentioned or elaborated on, but offer interesting hints at the possibility of radar signatures that are indicative of tornadogenesis.

Another paper, Cai (2005), compared the mesocyclones for both tornadic and non-tornadic supercells in attempt to show that it was possible to determine the difference between the two types of supercells using pseudovorticity calculations. Pseudovorticity is defined in the paper as being the difference between the maximum outbound velocity and maximum inbound velocity in the velocity couplet divided by the distance between the two maximum values.

$$\zeta_{pv} = \Delta V / L \qquad (1)$$

The prefix "pseudo" is used because equation (1) does not look at full vorticity and only measures vorticity along the radial of the radar beam. The study suggests that there will be notable differences between the slopes of the pseudovorticity lines, with the tornadic cases having a steeper slope than the non-tornadic cases. Even if pseudovorticity calculations are not used in the same way that it was used here, it can still be a useful diagnostic tool to determine the rotational strength of a velocity couplet.

As research into polarimetric variables continued, Van Den Broeke et al. (2008) looked at these radar products at different times during a given tornado's life cycle. That study defined certain high, medium, and low thresholds for reflectivity factor (Z_{HH}), differential reflectivity (Z_{DR}), specific differential phase (K_{DP}), and correlation coefficient (ρ_{hv}). With these defined thresholds, several tornadic supercells were analyzed visually during distinct times in the

tornado's life cycle. One rather interesting finding from that paper, with respect to tornadogenesis, is the presence of medium values of K_{DP} on the back side of the supercells that was only present in times prior to tornadogenesis. Considering that the study only looked at tornadic supercells, looking for this same signature in non-tornadic supercells could tell if this signature is indicative of tornadogenesis.

Two case studies (Houser et al. (2015) and Klees et al. (2016)) have also provided some insight into the life cycle of a tornadic supercell as well the differences between tornadic and non-tornadic supercells. Houser et al. (2015) found, using a mobile, rapid-scanning X-band, polarimetric Doppler radar (RaXPol), that storm scale processes, such as intensification and dissipation of velocity happened quite rapidly, in about 30s, but storm-scale processes that lead to tornadogenesis happened on the order of approximately 2 minutes. Another finding from that paper which could be particularly interesting is that tornadogenesis did not occur until after the strengthening of rotation between 3 and 3.5 km above ground. While that study did not look at non-tornadic supercells, this signature would be one that could be looked for when doing the comparison as it might potentially be a signature that is only visible in tornadic storms. In the second case study, Klees et al. (2016), it was found that non-tornadic supercells had strong rotation in the mid-levels, but weak low-level rotation, whereas the tornadic supercells had significant rotation both in the mid-levels and lower levels.

While the radar measurements in the previous two studies were taken from mobile X-band radars, these findings could prove very important in detecting tornadogenesis from WSR-88Ds. Considering that WSR-88Ds have a coarser temporal resolution when compared to the RaXPol radars, some of these features may happen too quickly to be resolved by the WSR-88D radars. However, other features should still be able to be resolved, especially with the implementation of Automated Volume Scan Evaluation and Termination (AVSET), Supplemental Adaptive Intra-Volume Low-Level Scans (SAILS), and Multiple Elevation Scan Option with SAILS (MESO-SAILS).

The intention of this research is to attempt to find a signature which appears in advance of tornadogenesis and does not appear in the non-tornadic cases; or find a signature which appears in the non-tornadic cases, but does not appear in the pre-tornadic cases. This research, then intends to determine the significance of any present signatures that fit these criteria and speculate on potential causes for these signatures.

2. Data and Methods

a. Data Selection

An initial set of days to search for potential pre-tornadic and non-tornadic supercells were selected based on the Storm Prediction Center (SPC) event archive. Days with reported tornadoes in the region of interest (Fig. 1) were selected from May 2013 to May 2016. Forty days were selected to search for potential cases. Following the selection of these potential case days, Next

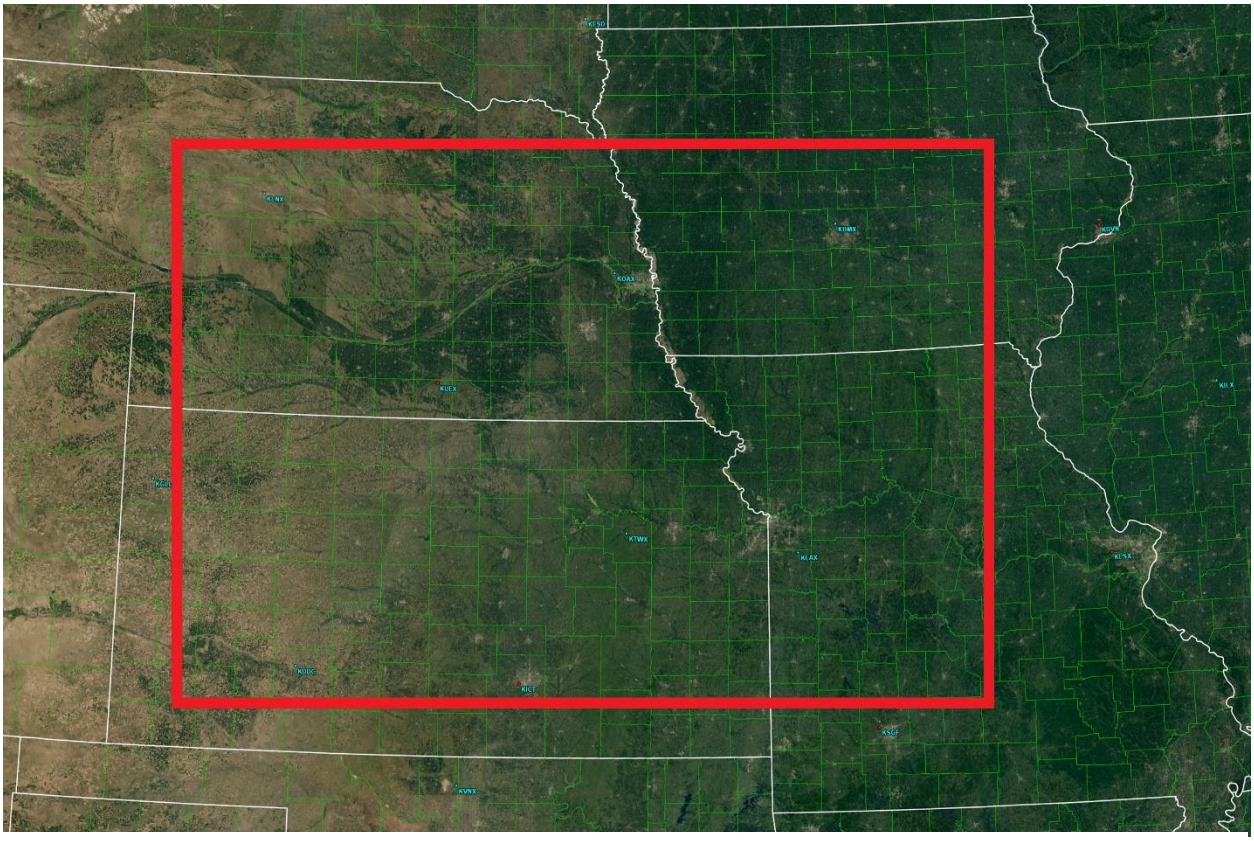

FIG. 1. The domain used for this study (inside of the red box).

Generation Radar (NEXRAD) Level II data was downloaded for the radar sites of interest from the National Center for Environmental Information (NCEI) Archive Information Request System (AIRS).

To begin refinement of this dataset, radar sites that did not have polarimetric data on the selected days were discarded, as the primary products this research looked at were polarimetric. A visual refinement of the radar data was then performed using GR2Analyst radar software. Cases that were too far from a radar, such that the lowest elevation tilt was 1.6 km or greater in elevation, or cases that were heavily contaminated by clutter, were discarded.

Since there are no databases which archive non-tornadic supercells, the next step in the data selection process was to determine whether a supercell was non-tornadic and, if it was, whether it was rotationally capable of producing a tornado as to avoid weakly rotating supercells. This was done in an attempt to ensure that the main factor limiting tornadogenesis was not rotational strength. Using the definition of a TVS (a gate-to-gate velocity difference of 46.3 m s^{-1} or greater over a distance of 1 km for velocity couplets within 56 km of the radar or a gate-to-gate velocity difference of 36.0 m s^{-1} over a distance of 1 km for velocity couplets over 56 km (National Weather Service 2009)), and using equation (1), the values of 0.0463 s^{-1} and 0.0360 s^{-1} were set as pseudovorticity thresholds for their respective distances from the radar. Supercells were then selected that were tornado warned with the "radar

TABLE 1. Non- and pre-tornadic cases used for this study. For the non-tornadic cases, the date and time at which the maximum pseudovorticity occurred is shown. For the pre-tornadic cases, the date and time which was closest to tornadogenesis is shown. Azimuth and range are measured from the radar site to the centroid of the velocity couplet.

a.) Non-Tornadic Cases				
Radar	Date and Time (UTC)	Azimuth (º)	Range (km)	Pseudovorticity (s^{-1})
KUEX	03 Oct 2013 02:30	76.0	89.1	0.0461
KICT	11 May 2014 02:07	79.0	85.7	0.0405
KICT	11 May 2014 05:34	75.5	106.8	0.0546
KDDC	08 May 2016 02:43	18.5	98.0	0.0737
KICT	25 May 2016 01:31	260.5	107.9	0.0523
b.) Pre-Tornadic Cases				
KOAX	16 Jun 2014 20:40	307.5	104.2	0.0270
KLNX	16 Jun 2014 23:19	103.5	104.6	0.0420
KLNX	18 Jun 2014 02:05	272.0	56.2	0.0782
KDMX	22 Jun 2015 22:05	141.5	80.3	0.0652
KOAX	09 May 2016 22:50	151.5	61.8	0.0354

indicated rotation" tag, which also had no discernable TDS and had no tornado reports. The pseudovorticities for each time step were then calculated using radial velocity in order to check to see if the supercell's velocity couplet ever met or exceeded the pseudovorticity thresholds. This further refined the dataset down to the five non-tornadic supercells that this study used (Table 1a).

Selecting the pre-tornadic supercells was much more simple, as SPC archives all tornado reports and local NWS offices perform damage surveys of suspected tornadoes. It was decided that, in order to keep the study consistent, five pre-tornadic supercells would be chosen to keep the datasets comparable (Table 1b). Once five storms were chosen, their pseudovorticities were also calculated to compare them to the non-tornadic supercells.

b. Visual Analysis

Once both pre- and non-tornadic datasets were defined, visual analysis was performed on both sets in an attempt to find a radar signature which was present in one type of supercell, but not the other. Both basic and polarimetric products were examined during this analysis. These products included reflectivity (Z_{HH}), spectrum width (σ_v), differential reflectivity (Z_{DR}), correlation coefficient (ρ_{hv}), and specific differential phase (K_{DP}) This study specifically focused on the lowest elevation tilt to look for these signatures, as this elevation tilt would be the closest to tornadic features.

c. Numerical and Statistical Analysis

Once a potential signature was found, the values for each gate in the signature were determined within the product in which it was found. This was done for each time step from fifteen minutes prior to tornadogenesis for

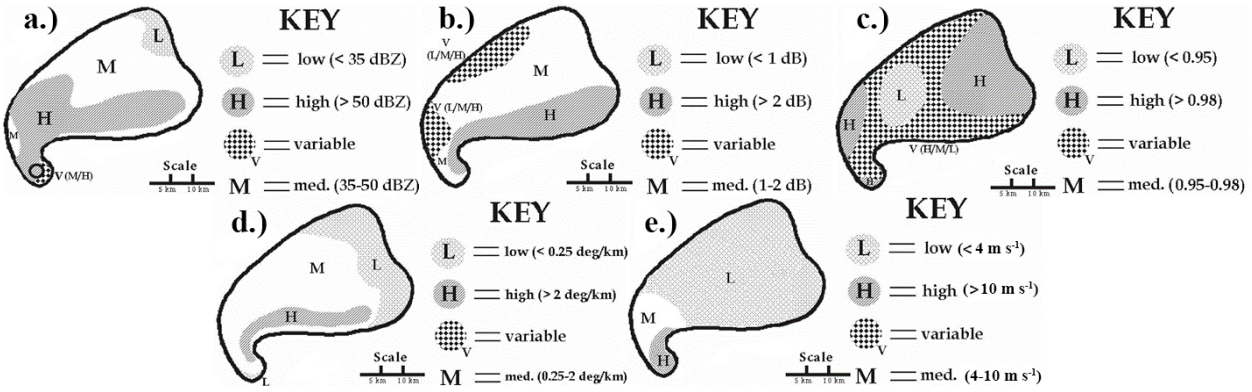

FIG. 2. An adapted version of the schematics created in Van Den Broeke et al. (2008) with an additional schematic created by this study for σ_v. These show pre-tornadic schematics for all of the basic and polarimetric products: a.) Z_{HH}, b.) Z_{DR}, c.) ρ_{hv}, d.) K_{DP}, and e.) σ_v. The key for each schematic is located to the right of the image. For all schematics, low values are the stippled areas, medium values are in the blank areas, high values are the hatched areas, and areas where values vary are represented by the checkerboard-filled areas. The thick black contour is representative of the 20 dBZ contour in Z_{HH}.

the pre-tornadic cases, or the maximum pseudovorticity value for the non-tornadic cases. Averages and standard deviations for the values of each time stamp, as well as the case average and standard deviation, were calculated in order to determine whether the signature was numerically visible. Further statistics were then performed using JMP Pro 12.

3. Results

a. Pseudovorticity analysis

As stated in data and methods, there are no databases which archive non-tornadic supercells, as they are not important to the general public and are basically only relevant in research. Due to this lack of an archive, determining a robust set of non-tornadic cases was essential for the validity of the findings of this study. Once an initial subset of non-tornadic supercells was selected using the methods specified in the previous section, these pseudovorticity values were calculated for both the pre- and non-tornadic cases using equation (1). Non-tornadic supercells that never surpassed the pseudovorticity thresholds for their respective range from the radar were discarded. A pooled t-test at the 95% confidence level was then performed on the pseudovorticity values of the remaining cases. This test was done for the values leading up to tornadogenesis or maximum pseudovorticity values to determine if there was any statistically significant difference in the pseudovorticity means for non-tornadic and pre-tornadic cases.

This t-test showed that there was not a statistically significant difference between the sets of pre- and non-tornadic supercells. This implies that pre- and non-tornadic supercells may share the same mean value, which is further supported when looking at the means for each. The pre-tornadic mean pseudovorticity value was 0.0340 s^{-1} and the

non-tornadic mean pseudovorticity value was 0.0320 s^{-1}. However, this finding does show that the selection process was able to select a set of cases that were relatively similar in rotational strength during storm intensification, suggesting that something other than rotation is limiting tornadogenesis in the non-tornadic cases. For the full t-test and means, see the appendix at the end of the study.

b. Analysis of radar products

Using the pre-tornadic thresholds defined in Van Den Broeke et al. (2008) for Z_{HH}, Z_{DR}, ρ_{hv}, and K_{DP}, as well as setting threshold values for σ_v (Fig. 2e), visual analysis was performed using GR2Analyst radar software on the ten cases for the fifteen minutes preceding tornadogenesis for the pre-tornadic cases and maximum pseudovorticity for the non-tornadic cases. The observed values were then compared to the predefined thresholds in Van Den Broeke et al. (2008). Any differences from the threshold values or differences in location of certain values (Fig. 2) were noted, and any consistent differences from these were investigated further in the analysis.

Both pre- and non-tornadic cases mostly followed the schematic for Z_{HH}, with the exception of the 16 June 2014 pre-tornadic supercell observed by the Omaha, Nebraska (KOAX) WSR-88D (Fig. 3). This storm had more of an amorphous appearance with two potential hook echoes on the east side of the storm; only one of which had rotation. Regardless of this lack in supercell structure, it went on to produce the Stanton, Nebraska EF4 tornado and the Pilger, Nebraska twin EF4 tornadoes. All other cases showed the more classic supercell appearance. All cases exhibited a hook echo which became increasingly cyclonically curved, to varying

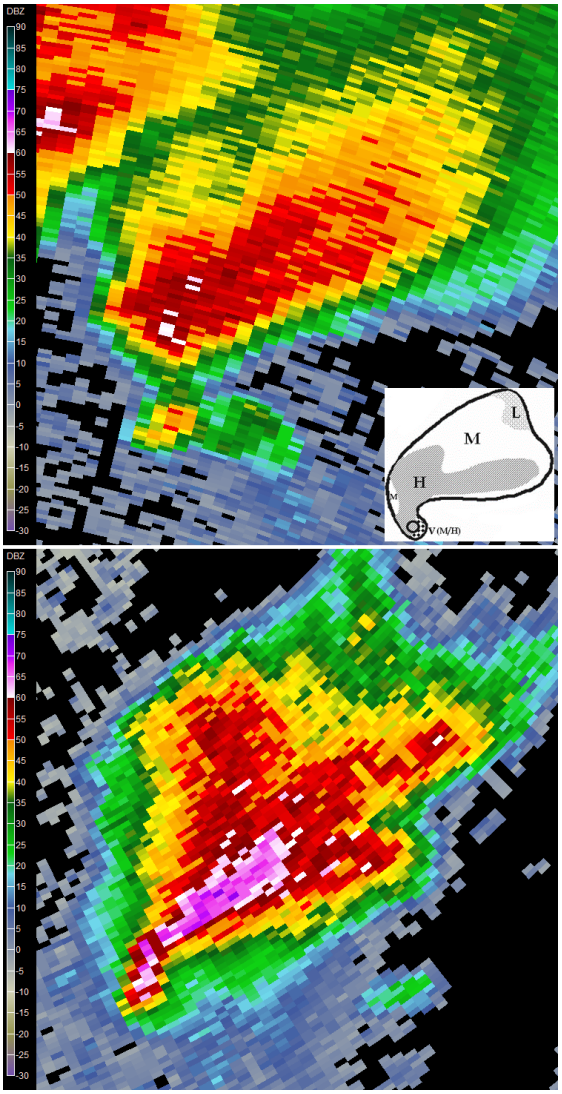

FIG. 3. This shows Z_{HH} for both non-tornadic and pre-tornadic cases 7 minutes prior to the maximum pseudovorticity value for the non-tornadic case and tornadogenesis for pre-tornadic case. The 09 May 2016 KDDC non-tornadic supercell is at the top, the 09 May 2016 KOAX pre-tornadic supercell is at the bottom, and the Van Den Broeke et al. (2008) schematic for Z_{HH} is at the bottom right corner of the top image. Units are in dBZ.

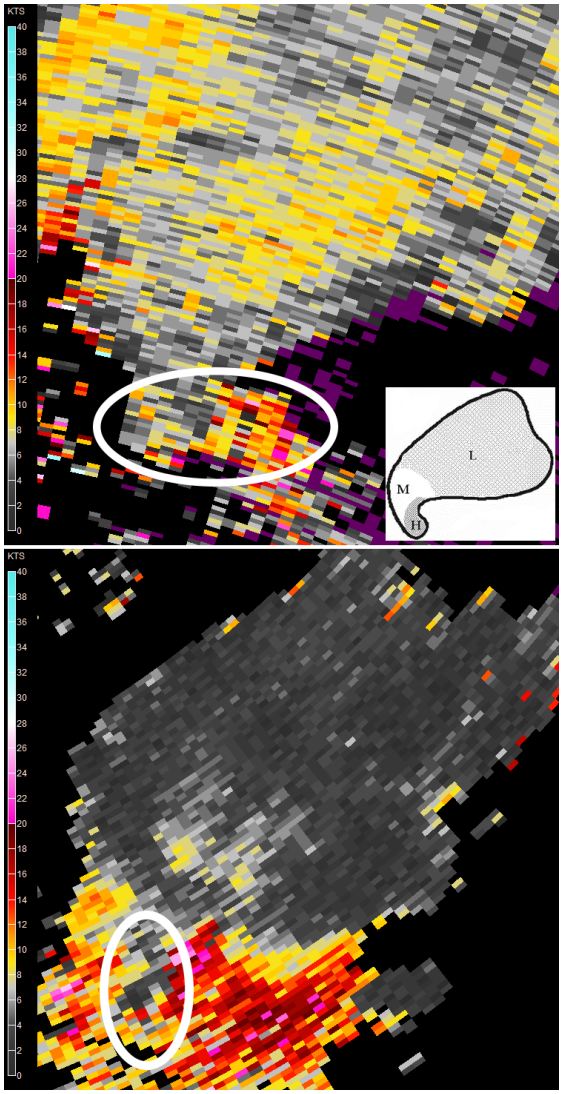

FIG. 4. Same as what is shown in Fig. 3, but for σ_v. The areas circled in white are the hook echo regions of each storm. Units for this plot are in knots.

extents, as the supercells intensified. Some supercells had visible descending reflectivity cores (DRC), however these were present in some form in both the pre- and non-tornadic cases. One supercell in particular, 22 June 2015, observed by the Des Moines, Iowa (KDMX) WSR-88D underwent tornadogenesis very shortly after a DRC interacted with the supercell. This lends credence to studies such as Rasmussen et al. (2006) which, in the cases observed, found that DRC descent happened prior to tornadogenesis. However, since these DRCs were present in both the pre- and non-tornadic supercells observed in this study, they were not looked at further.

Values for σ_v varied slightly from storm to storm (Fig. 4). The highest values for all cases were found in the area where the velocity couplet was present. This makes sense as there is a significant amount of turbulent motion in the velocity couplet. Several cases had very uniform low values for the rest of the areal extent of their supercells, while others had medium values along the forward flank and in the area of highest Z_{HH} (Fig. 2e). Even the cases which had these medium values had low values along the periphery of their supercell. No discernable pattern was apparent to the author as these discrepancies in σ_v did not seem to favor the pre- or the non-tornadic cases. Due to this, σ_v was not evaluated further than the visual analysis.

The pre-tornadic cases followed the schematic for Z_{DR} for the most part, with the exception of the hook echo (Fig. 5). In the schematic for Z_{DR}, the values in the hook echo of the pre-tornadic cases is between medium and high (Fig. 2b). However, in four of the five cases analyzed, the hook echo had medium to low values for the pre-tornadic cases. The one case that did not follow this pattern was the 16 June 2014 supercell observed by the KOAX WSR-88D; the amorphous supercell mentioned in the discussion of Z_{HH}. This case ended up having the highest Z_{DR} values in the hook echo of any of the ten cases observed. The non-tornadic

cases followed the schematic more closely, as these cases appeared to have higher Z_{DR} values in the hook echo than the pre-tornadic cases. Other than the discrepancy in the hook echoes, Z_{DR} appeared to follow the Van Den Broeke et al. (2008) schematics well, with high values along the forward flank, decreasing to medium values towards the rear of the supercells. Some storms with higher Z_{HH} values also had lower Z_{DR} in these areas. This is to be expected as hail is probable in these locations and the tumbling nature of hail causes Z_{DR} to approach zero while Z_{HH} increases. Since the discrepancy between hook echo values of Z_{DR} appears to be specific to whether the supercell is pre- or non-tornadic, this signature was investigated further with statistical analysis.

When comparing ρ_{hv} for both pre- and non-tornadic supercells to the Van Den Broeke pre-tornadic schematic (Fig. 2c), both appeared to follow it pretty much exactly early on (Fig. 6). With that said, later in the intensification process, still prior to maximum pseudovorticity or tornadogenesis, the ρ_{hv} fields began to resemble the schematic for an ongoing tornado with the lack of extremely low ρ_{hv} values in the hook echo. These extremely low ρ_{hv} values are caused by debris lofted by an ongoing tornado (Stelten and Wolf 2014). Since the ρ_{hv} fields for both pre- and non-tornadic appeared to be mostly uniform throughout all cases, ρ_{hv} was not evaluated further.

In Van Den Broeke et al. (2008), a signature of medium K_{DP} values appeared along the back side of the supercell only in pre-tornadic times, which dissipated when going into tornado time, as mentioned in the

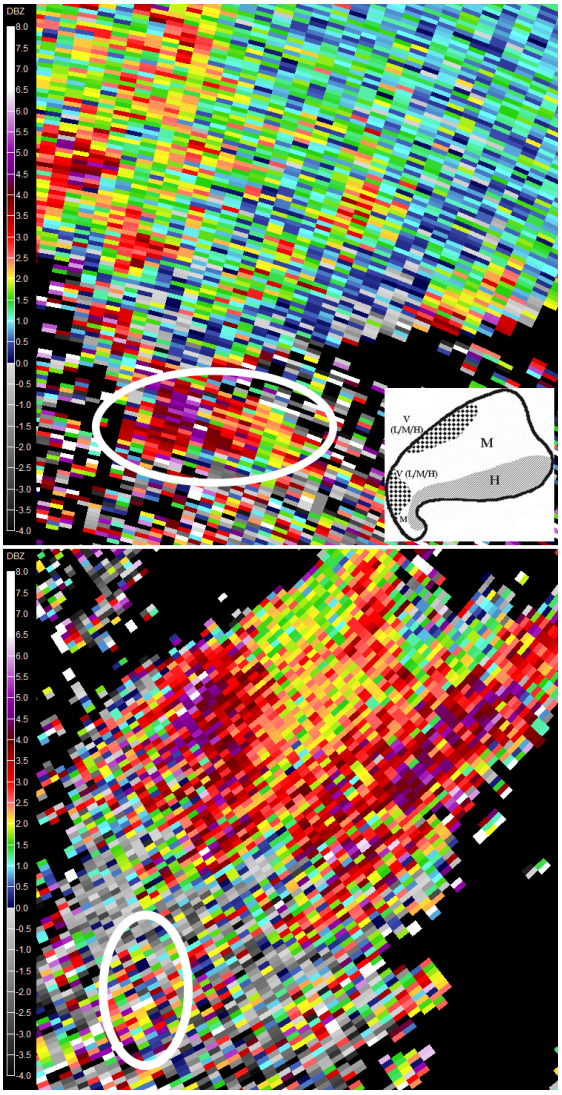

FIG. 5. Same as what is shown in Fig. 4, but for Z_{DR}. Units are in dBZ.

introduction of this research (Fig. 2d). The meaning of this signature was cautiously speculated about in that paper. Considering that this signature appeared only during pre-tornadic times, it made for a great candidate to search for during visual analysis of K_{DP} due to the slight possibility that it could be indicative of tornadogenesis. However, in this study, both pre- and non-tornadic supercells had issues following the schematic. Several followed it almost

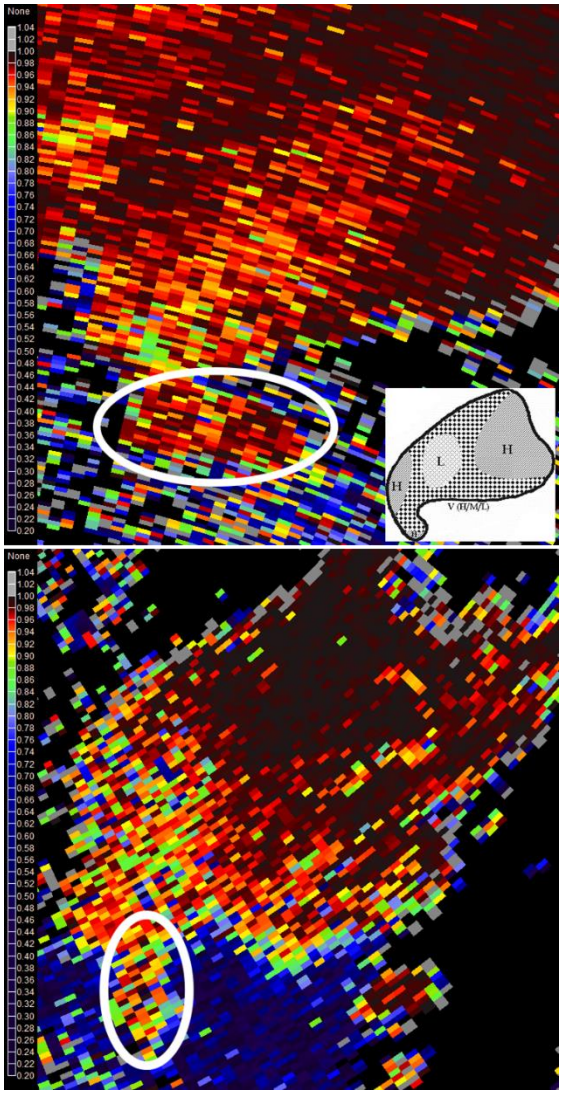

FIG. 6. Same as what is shown in Fig. 5, but for ρ_{hv}. Quantities do not have units.

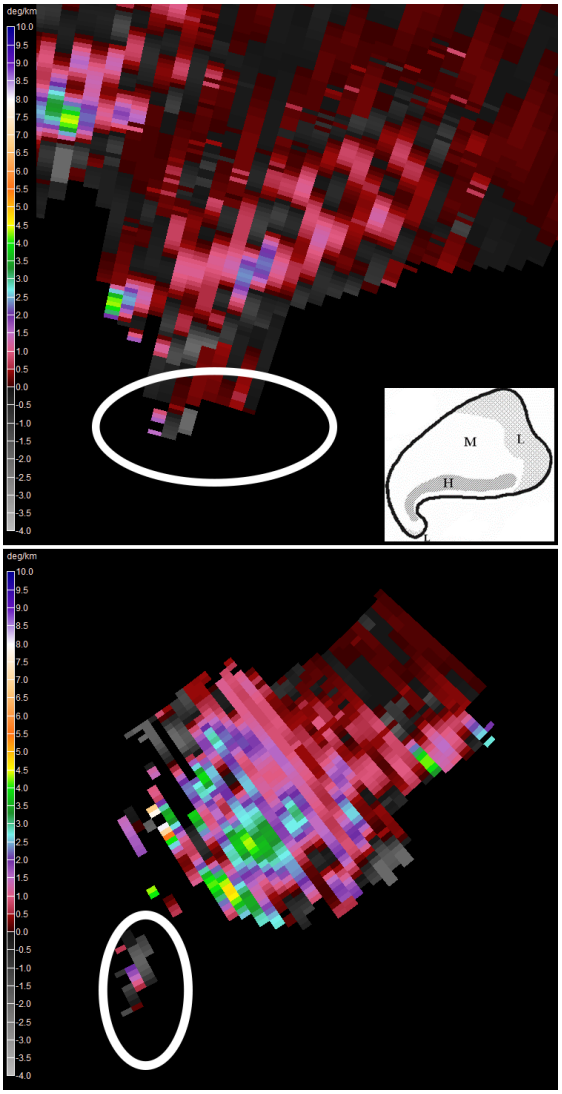

FIG. 7. Same as what is shown in Fig. 6, but for K_{DP}. Units are ^{o} km^{-1}.

exactly, but others had much larger areas of high K_{DP} values (Fig. 7). There was not any discernable bias for which type of case would not follow the schematic well, as a mixture of pre- and non-tornadic cases had this issue. The medium values specified along the back side of the supercells were present in both pre- and non-tornadic cases. Due to this, that signature was not investigated statistically.

c. Statistical analysis of Z_{DR} signature

There was one signature in Z_{DR} that appeared to differ only depending on whether the case was pre- or non-tornadic. In the pre-tornadic cases, there were medium to low Z_{DR} values present in the hook echo and in the non-tornadic cases, there were medium to high values of Z_{DR} present. To determine whether this signature was numerically present in the data, the Z_{DR} value for each gate in the hook echo was recorded for all of

TABLE 2. The mean, standard deviation, and variance of Z_{DR} calculated for the non- and pre-tornadic cases used for this study. All units are in dBZ. The 16 Jun 2014 case was considered a major outlier. Hence the reasoning for calculating the variance with and without that case. The averages were calculated for all time steps 15 minutes prior to the maximum pseudovorticity value or tornadogenesis up until those respective times.

a.) Non-Tornadic Cases				
Radar	Date	Case Avg.	Case S. Dev.	Variance of all cases
KUEX	03 Oct 2013	1.57	0.86	1.59
KICT	11 May 2014	1.95	1.29	
KICT	11 May 2014	2.03	1.02	
KDDC	08 May 2016	3.10	1.38	
KICT	25 May 2016	2.43	0.99	
b.) Pre-Tornadic Cases				
KOAX	16 Jun 2014	3.85	0.78	2.06
KLNX	16 Jun 2014	1.52	1.18	
KLNX	18 Jun 2014	1.87	1.25	
KDMX	22 Jun 2015	1.06	0.69	
KOAX	09 May 2016	0.80	1.60	
c.) Pre-Tornadic Cases without 16 Jun 2014 KOAX				
KLNX	16 Jun 2014	1.52	1.18	1.57
KLNX	18 Jun 2014	1.87	1.25	
KDMX	22 Jun 2015	1.06	0.69	
KOAX	09 May 2016	0.80	1.60	

the pre- and non-tornadic cases. These values were recorded for all time steps from fifteen minutes prior to either tornadogenesis or maximum pseudovorticity value up until those respective times were reached. The averages and standard deviations were then calculated for each case (Table 2).

From this, it became more apparent that this signature could be numerically present. Most of the averages for the pre-tornadic cases were lower than the non-tornadic cases, with the exception of a slight overlap in a couple of cases as well as the very apparent outlier of the 16 June 2014 pre-tornadic supercell observed by the KOAX WSR-88D (Table 2b). Even so, the variances for all of the pre- and non-tornadic Z_{DR} values were calculated to ensure that they satisfied the assumption for the pooled t-test. The variance for the pre-tornadic Z_{DR} values without the KOAX outlier supercell was also calculated to ensure that the assumption for the pooled t-test was also valid (Table 2c). This was done so that the pooled t-test could be done to compare the means of the pre- and non-tornadic Z_{DR} values with and without the outlier to see what sort of difference the outlier made.

With the pooled t-test variance condition satisfied for comparing with and without the

TABLE 3. The mean of all values of Z_{DR} for a particular case type, the lower and upper bounds of the 95% confidence interval, and the t-test probability that the mean of the pre-tornadic cases (both with and without the outlier) would be greater than the mean of the non-tornadic cases.

Results of the Pooled t-test				
Case Type	Avg Z_{DR}	Lower 95% CI	Upper 95% CI	t-test Probabilities
All Non-Tornadic	2.23	2.19	2.27	N/A
All Pre-Tornadic	1.79	1.74	1.84	< 0.0001
Pre-Tornadic w/o outlier	1.49	1.44	1.54	< 0.0001

outlier case, the t-test at the 95% confidence level was performed. For the comparison with the outlier included, the test clearly showed statistically significant evidence that the two means were not equal. This suggests that there is a statistically significant difference between the two means with the pre-tornadic Z_{DR} values having a lower mean than the non-tornadic Z_{DR} values. This confirms the visual analysis that there is indeed a difference, at least in these ten cases, between pre- and non-tornadic Z_{DR} values in the hook echo. To see how much the outlier may have affected this statistic, the pooled t-test without the outlier was done. This t-test further confirmed what the previous one had shown. The test clearly showed statistically significant evidence that the two means were not equal, thus suggesting a difference in the means, with pre-tornadic cases having the smaller mean Z_{DR} (Table 3). As with the pseudovorticity t-test, the full t-tests are included in the appendix.

4. Conclusion and Discussion

For the ten cases looked at in the study, there is a strong statistically significant difference between the mean values of Z_{DR} in the hook echoes of pre- and non-tornadic supercells. The signature is not always easy to pick up visually due to the high values associated with DRCs, especially during interaction between DRCs and the parent supercell. It does show up more easily when the mean of all gates within the hook echo is taken. This offers the suggestion of a possibility for this signature to have a relationship in some way with tornadogenesis. Due to the small sample size used in the study, investigating more cases will provide more concrete evidence as to the usefulness and reliability of this signature. Polarimetric capability has only been available in the domain of interest for, at most, three years for the WSR-88Ds. This, in tandem with the below average severe weather seasons over the past three years, lead to this small sample size.

Physically, without some form of ground observations or in-situ data, it is difficult to know exactly what could be causing this signature. The author's first thought on what could potentially be causing the signature is that, for some reason in the non-tornadic case, there are much larger hydrometeors in the hook echo region of the storm than in the pre-tornadic case. This could be due to how size sorting of hydrometeors occurs in one case verses the other. Z_{HH} values in the hook echo of each are relatively similar in both pre- and non-tornadic storms. Therefore, if there were larger hydrometeors present in the non-

tornadic case, there would have to be less of them to account for the lack of difference in Z_{HH} (Ryzhkov et al. 2005). This could potentially suggest that, if the hydrometeors in the pre-tornadic case are indeed smaller, that there could be more evaporative cooling ongoing in the hook echo of the pre-tornadic supercell. This could enhance the storm's rear flank downdraft (RFD) and therefore increase the chance of tornadogenesis. However, the issue with this idea is that most RFDs tend to be warm, not cold, so further analysis of this is necessary to understand the ongoing processes involved.

Further study of this Z_{DR} signature is necessary in order to fully understand the usefulness and reliability of it. Now, with the implementation of AVSET, SAILS, and MESO-SAILS, the higher temporal resolution of low level radar scans should also be able to give more insight into this signature after a few years, once a larger set of cases can be obtained. This study had two cases with MESO-SAILS, five cases with SAILS, and three cases with neither.

The outlier case, the 16 June 2014 supercell observed by KOAX could prove to be interesting for this signature, as it produced large, long track tornadoes, but the Z_{DR} values in the hook echo were higher than any other case, pre- or non-tornadic. Aside from this supercell, the other four pre-tornadic cases Z_{DR} values fit the pattern observed well with only slight overlap into the non-tornadic cases values (Fig. 8). Dividing the pre- and non-tornadic storms up into low precipitation, high precipitation, classic supercells, or other types such as quasi-linear convective systems (QLCS) or mesoscale convective vortices (MCV), to see if the signature is more prevalent in certain cases more than others could potentially lead to explaining the outlier case, as well as refining which situations the signature could be useful for.

Acknowledgements. The author would like to thank several individuals for their help during the process of this research. Dr. Rachindra Mawalagedara for her help with the writing process of the background information and the paper itself. Dr. William Gallus for his insight on what thresholds to use to classify the non-tornadic cases. Sean Stelten for helping the author work through the storm scale processes that could potentially be ongoing. Dr. James Aanstoos for his help with the radar product insight, help with deciding what sort of testing should be done on the found signature as well as being a very helpful mentor.

REFERENCES

Cai, H., 2005: Comparison between tornadic and nontornadic mesocyclones using the vorticity (pseudovorticity) line technique. *Mon. Wea. Rev.*, **133**, 2535-2551.

Houser, J. A., H. B. Bluestein, J. C. Snyder, 2015: Rapid-scan, Polarimetric, Doppler radar observations of tornadogenesis and tornado dissipation in a tornadic supercell: The "El Reno, Oklahoma" storm of 24 May 2011*. *Mon. Wea. Rev.*, **143**, 2685-2710.

Klees, A. M., Y. P. Richardson, P. M. Markowski, C. Weiss, J. M. Wurman, K. K. Kosiba, 2016: Comparison of the tornadic and nontornadic supercells intercepted by VORTEX2 on 10 June 2010. *Mon. Wea. Rev.*, **144**, 3201-3231.

National Weather Service, 2009: Glossary; Tornado Vortex Signature. Accessed 24 September 2016 [Available online at http://w1.weather.gov/glossary/index.php?word=tornado+vortex+signature]

Rasmussen, E. N., J. M. Straka, M. S. Gilmore, R. Davies-Jones, 2006: A preliminary survey of rear-flank descending reflectivity cores in supercell storms. *Wea. Forecasting.*, **21**, 923-938

Ryzhkov, A. V., T. J. Schuur, D. W. Burgess, D. S. Zrnic, 2005: Polarimetric tornado detection. *J. Appl. Meteor.*, **44**, 557-570.

Stelten, S., and R. Wolf, 2014: Investigating the effect of land cover on the correlation between TDS heights and tornado strength and other TDS characteristics. Abstract, *18th Annual Severe Storms and Doppler Radar Conf.*, Ankeny, IA, National Weather Association Central Iowa Chapter. [Available online at http://www.iowa-nwa.com/conference/files/2014_Agenda_Lite.pdf.]

Van Den Broeke, M. S., J. M. Straka, E. N. Rasmussen, 2008: Polarimetric radar observations at low levels during tornado life cycles in a small sample of classic Southern Plains supercells. *J. Appl. Meteor. Climatol.*, **47**, 1232-1247.

APPENDIX

APPENDIX A. This table shows the full t test analysis for the all non-tornadic and pre-tornadic pseudovorticity values

t Test			
PreTornadic-NonTornadic			
Assuming equal variances			
Difference	0.00195	t Ratio	0.491728
Std Err Dif	0.00397	DF	61
Upper CL Dif	0.00988	Prob > |t|	0.6247
Lower CL Dif	-0.00598	Prob > t	0.3123
Confidence	0.95	Prob < t	0.6877

Level	Number	Mean	Std Error	Lower 95%	Upper 95%
NonTornadic	33	0.031933	0.00274	0.02646	0.03741
PreTornadic	30	0.033884	0.00287	0.02814	0.03962

APPENDIX B. This table shows the full t test analysis for the all non-tornadic cases and all pre-tornadic cases.

t Test			
PreTornadic-NonTornadic			
Assuming equal variances			
Difference	-0.44126	t Ratio	-14.3892
Std Err Dif	0.03067	DF	7945
Upper CL Dif	-0.38115	Prob > |t|	<.0001*
Lower CL Dif	-0.50138	Prob > t	1.0000
Confidence	0.95	Prob < t	<.0001*

Level	Number	Mean	Std Error	Lower 95%	Upper 95%
Non-Tornadic	4863	2.22939	0.01910	2.1919	2.2668
Pre-Tornadic	3084	1.78812	0.02399	1.7411	1.8351

APPENDIX C. This table shows the full t test analysis for the all non-tornadic cases and pre-tornadic cases without the one outlier case.

t Test			
PreTornadic-NonTornadic			
Assuming equal variances			
Difference	-0.73740	t Ratio	-24.3919
Std Err Dif	0.03023	DF	7559
Upper CL Dif	-0.67814	Prob > |t|	<.0001*
Lower CL Dif	-0.79666	Prob > t	1.0000
Confidence	0.95	Prob < t	<.0001*

Level	Number	Mean	Std Error	Lower 95%	Upper 95%
NonTornadic	4863	2.22939	0.01806	2.1940	2.2648
PreTornadic	2698	1.49199	0.02424	1.4445	1.5395